Research Square

Preprints are preliminary reports that have not undergone peer review.
They should not be considered conclusive, used to inform clinical practice,
or referenced by the media as validated information.

No detectable inflection point in U.S. oil and gas methane emissions following the Inflation Reduction Act

Ao Chen

achen152@jh.edu

Johns Hopkins University https://orcid.org/0000-0002-3604-3403

William Daniels

Johns Hopkins University https://orcid.org/0000-0001-8752-5536

Ziting Huang

Johns Hopkins University

Arvind Ravikumar

The University of Texas at Austin https://orcid.org/0000-0001-8385-6573

Sarah Jordaan

McGill University https://orcid.org/0000-0002-1277-4746

Zhen Zhang

Institute of Tibetan Plateau Research, Chinese Academy of Sciences

Leyang Feng

Johns Hopkins University

Hanyu Liu

Johns Hopkins University

Lee Murray

University of Rochester https://orcid.org/0000-0002-3447-3952

Xueying Yu

State University of New York at Albany

Dylan Gaeta

Cooperative Institute for Research in Environmental Sciences (CIRES) https://orcid.org/0000-0001-5186-3197

Kristan Morgan

Johns Hopkins University

Jialuo Yuan

Stanford University

Scot Miller

Johns Hopkins University https://orcid.org/0000-0003-4462-8126

Article

Keywords: Inflation Reduction Act, methane emissions, oil and gas, Waste Emission Charge

Posted Date: April 8th, 2026

DOI: https://doi.org/10.21203/rs.3.rs-9295605/v1

License: This work is licensed under a Creative Commons Attribution 4.0 International License.
Read Full License

Additional Declarations: There is **NO** Competing Interest.

Version of Record: A version of this preprint was published at Communications Earth & Environment on October 13th, 2026. See the published version at https://doi.org/10.1038/s43247-026-04039-0.

No detectable inflection point in U.S. oil and gas methane emissions following the Inflation Reduction Act

Ao Chen[1*], William S. Daniels[1], Ziting Huang[1], Arvind P. Ravikumar[2], Sarah M. Jordaan[3], Zhen Zhang[4], Leyang Feng[1], Hanyu Liu[1], Lee T. Murray[5], Xueying Yu[6], Dylan C. Gaeta[1], Kristan L. Morgan[1], Jialuo Yuan[7], Scot M. Miller[1*]

[1]Department of Environmental Health and Engineering, Johns Hopkins University, Baltimore, MD, 21205, USA.
[2]Hildebrand Department of Petroleum and Geosystems Engineering, The University of Texas at Austin, Austin, TX, 78712, USA.
[3]Department of Civil Engineering, McGill University, Montreal, Quebec, H3A 0C3, Canada.
[4]National Tibetan Plateau Data Center (TPDC), State Key Laboratory of Tibetan Plateau Earth System, Environment and Resource (TPESER), Institute of Tibetan Plateau Research, Chinese Academy of Sciences, Beijing, 100101, China.
[5]Department of Earth and Environmental Sciences, University of Rochester, Rochester, NY, 14627, USA.
[6]Atmospheric Sciences Research Center, State University of New York at Albany, Albany, NY, 12226, USA.
[7]Department of Civil and Environmental Engineering, Stanford University, Stanford, CA, 94305, USA.

*Corresponding author(s). E-mail(s): achen152@jh.edu; smill191@jhu.edu;

Abstract

The U.S. federal government undertook a flurry of new actions to monitor and regulate methane emissions beginning in years 2021 and 2022, including the Inflation Reduction Act (IRA). The IRA and Waste Emissions Charge (WEC)

represent a historic legislative effort to regulate U.S. methane emissions, yet its early effectiveness remains empirically unverified. Here we estimate changes in U.S. oil and gas methane emissions during 2019–2024 using an inverse model constrained by satellite observations. We find no detectable inflection point in U.S. oil and gas methane emissions in the years following these legislative and regulatory actions. Although methane emissions intensity from the oil and gas sector declined by 9.3–13.6% during 2019–2024, this trend likely reflects gradual technological, operational, and regulatory developments rather than any abrupt shift associated with federal policy. Furthermore, we identify a divergence in inventory reliability: state-level inventories align with satellite estimates in the highest emitting states with greenhouse gas (GHG) emission targets but underestimate emissions by a factor of about 4 in the highest emitting states without GHG targets. Our results underscore the limitations of transient legislative signals, suggesting that without long-term regulatory durability, the industry lacks the incentive to commit to methane emission reductions.

Keywords: Inflation Reduction Act, methane emissions, oil and gas, Waste Emission Charge

Main

The Inflation Reduction Act (IRA), enacted in August 2022, represents the first legislation passed by the U.S. Congress to directly regulate methane emissions. The IRA introduced the Waste Emissions Charge (WEC), to be assessed beginning in 2024, and allocated substantial funding to accelerate methane detection, measurement, and mitigation technologies [1]. Specifically, as the first federally imposed fee on methane emissions, the WEC was widely seen as creating a financial incentive that would drive reductions in U.S. methane emissions [2]. The IRA further established the Methane Emissions Reduction Program, allocating $1.36 billion to provide technical and financial support to the oil and gas (O&G) sector [3]. In 2021, the White House also asked the Environmental Protection Agency (EPA) to begin a rulemaking process for methane emissions from new and existing sources using its authority under the Clean Air Act [4], and the EPA finalized these rules in 2024 [5]. As part of these rules, the EPA finalized regulations for both new and existing O&G sources, specifically issuing New Source Performance Standards (NSPS) Subpart OOOOb for new or modified infrastructure and Emission Guidelines (EG) Subpart OOOOc for existing facilities [6] (see Table S1 for timelines of all U.S. methane regulations related to NSPS, IRA, and WEC).

Given the comprehensive scale of these provisions, the IRA and EPA rules were widely anticipated to function as a formidable regulatory signal, potentially driving a detectable inflection point in U.S. methane emission trends. However, these emissions reductions may not have been realized, both due to delays in implementing the WEC and EPA rules (see Table S1), and due to political actions in Washington beginning in 2025 that have made these measures effectively null and void [1]. For example, Congress nullified the EPA's WEC rule in early 2025 [7]. The White House also repealed the Endangerment Finding in early 2026, which underpinned many previous GHG

regulations, including EPA's methane rules [8]. Beyond federal action, however, many U.S. states (see Table S2) have set explicit GHG emissions reduction goals [9], and state action could yield a decrease in emissions irrespective of federal regulation [10].

In this study, we aim to estimate changes in Contiguous U.S. (CONUS) methane emissions between years 2019 and 2024, particularly from the O&G sector, using TROPOMI satellite observations. We develop a regional inverse model using these observations and estimate emissions at a daily time resolution and a spatial resolution of 0.5° latitude by 0.625° longitude. To date, few studies have quantified changes in U.S. O&G methane emissions following the IRA using atmospheric-based measurements. This research gap leaves the influence of federal methane policy largely untested, especially in the O&G sector, where companies may have proactively taken steps to comply with the IRA during its initial roll out. We hypothesize that the methane-related provisions of the IRA have not yielded a detectable inflection point in U.S. methane emissions to date, likely owing to political turnover and delays in federal implementation, whereas well-established state-level regulations and methane emission targets (e.g., California and Colorado) had a positive effect on methane emissions monitoring and reduction.

Emissions intensity declines despite no clear impact of IRA

We do not observe an inflection point in O&G methane emissions or in emission intensity in the years following the IRA (Fig. 1). In fact, we find that O&G methane emissions increased by 0.21 [-0.06, 0.53] Tg from 2023 to 2024, where the provided uncertainty is the range of our inverse modeling ensemble (see Table 1). This lack of inflection point following the IRA is perhaps unsurprising given two details of its implementation, or lack thereof. First, the IRA established the WEC, beginning at $900 per ton in 2024 and increasing to $1500 per ton in 2026, but most implementation details – such as conditional exemptions, monitoring requirements, and the EPA's final methane regulations [7]– remained unsettled through 2026. Consequently, the WEC was not yet functionally active during the study period, meaning that the primary economic levers intended to catalyze immediate new actions or emission efforts by O&G companies had not yet materialized. Even if the WEC were fully implemented, however, the EPA projected that it would have only a nominal impact on methane emission – an annual reduction of 0.15 Tg year^{-1} in 2024, and a cumulative reduction of just 0.96 Tg over the entire 2023–2035 period[7, 12, 13]. Second, EPA's new methane rules (OOOOc) for existing O&G facilities have also not come into effect. These rules would have superseded the WEC for compliant facilities, and unlike the WEC, the EPA projected that they would have had a large impact on emissions – an annual reduction of about 4 Tg year^{-1}, equivalent to ∼40% of our annual estimate for U.S. O&G methane emissions (Table 1-3 in EPA[14]). However, no states submitted State Implementation Plans (SIP) by 2024 before the scheduled onset of WEC charges, and in early 2025, the new White House delayed enforcement and implementation of these EPA rules (see Table S1 for details).

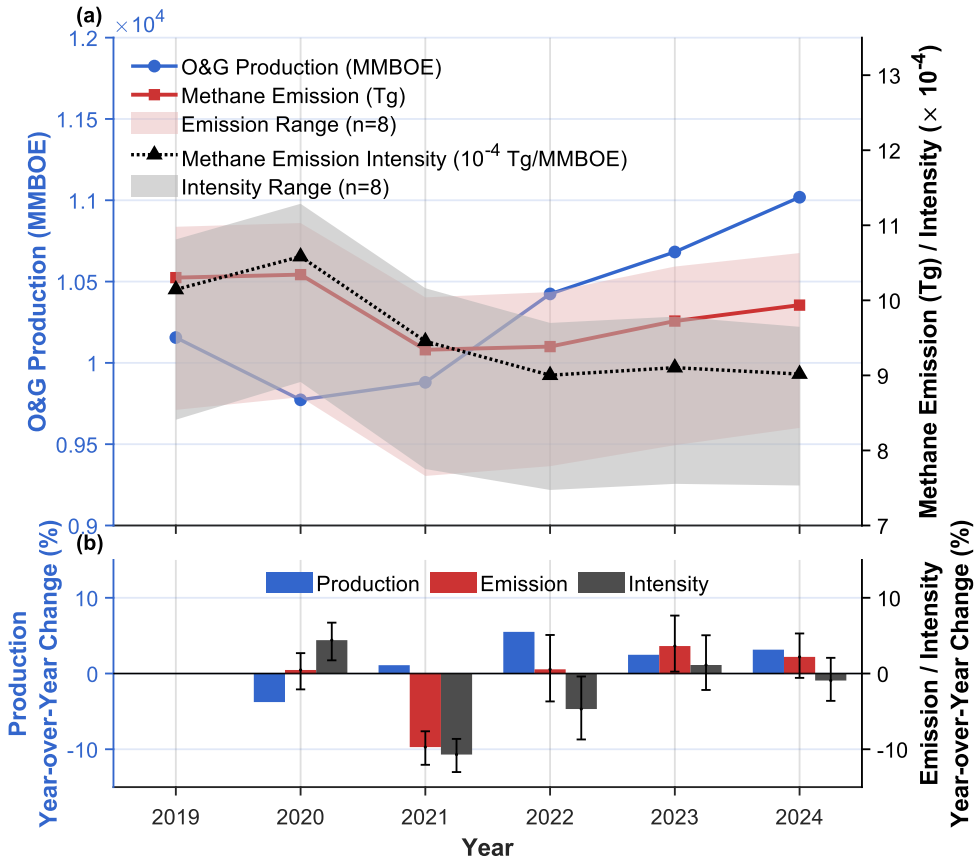


Fig. 1 (a) Trends in U.S. O&G production, methane emissions, and emission intensity during 2019–2024. Methane emission intensity is defined here as total O&G methane emissions divided by total O&G production. Total O&G production (solid blue line, left y axis) is shown in million barrels of oil equivalent (MMBOE) per year, with natural gas converted using an energy equivalence of 6,000 cubic feet per barrel [11]. Average methane emissions (solid red line, right y axis) represent the average of 8 scenarios (see Table 1, same below), with the red shaded area indicating the full range (minimum to maximum) in 8 scenarios. Average methane intensity (dashed black line; 10^{-4} Tg/MMBOE) and the gray shaded area denote the ratio of average emissions to total production and its associated uncertainty. The intensity uncertainty is derived from the full range (minimum to maximum) in our methane emissions estimates. (b) Year-over-year percentage changes. Vertical error bars denote the full ensemble range (minimum to maximum) derived from the 8 scenarios.

A lack of inflection point in U.S. methane emissions surrounding the IRA is likely also a result of varying corporate responses to the pending regulatory framework. While a subset of large, forward-looking operators had already proactively initiated enhanced monitoring and assessment protocols when the IRA passed [15], many others maintained a cautious "wait-and-see" posture as the technicalities of the WEC and its alignment with EPA methane rules evolved [16]. Even some proactive firms implemented strategic pauses in late 2023 to assess how the WEC would interact with the EPA rules [16].

Although we do not see a clear inflection point in U.S. O&G methane emissions during our study period, we cannot rule out year-to-year changes in emissions below the detection limit of our inverse model. We estimate a year-to-year ensemble detection limit of approximately 0.35 Tg yr^{-1}, defined as 2σ of the ensemble variability (see SI). An even more conservative estimate for this quantity is 0.60 Tg yr^{-1}, defined as the full ensemble range width (see SI). In addition, we cannot rule out a counterfactual scenario where emissions would have risen more than 0.21 Tg in the absence of the IRA and other EPA regulatory activities; thus, our inverse model results may represent a "mitigated growth" emissions scenario rather than a complete lack of impact by the IRA. We also note that the attribution of emissions to individual sectors is an additional source of uncertainty and is discussed in detail in the Methods and Supporting Information.

We find a longer-term decline in U.S. O&G methane emissions intensity, even though we do not see a clear inflection point in O&G emissions concurrent with the IRA. Specifically, we find that emissions intensity from the O&G sector in CONUS declined by approximately 11.1% [9.3%, 13.6%] from 2019 to 2024, from 10.1 [8.4, 10.8] 10^{-4} Tg $MMBOE^{-1}$ in 2019 to 9.0 [7.5, 9.6] 10^{-4} Tg $MMBOE^{-1}$ in 2024. Although most of this decline in intensity occurred between 2020 to 2022, it represents, on average, a 2.2% [1.9%, 2.7%] decline in intensity per year. This result suggests a slowing decline in U.S. O&G methane emissions intensity, as Lu et al. [17] found a 32% reduction in emissions intensity between 2010 and 2019, or, on average, a 3.6% decline per year.

The decline in O&G emissions intensity is concurrent with a 8.5% increase in production from 2019 to 2024 (Fig. 1) and is in line with basin-specific satellite inverse model estimates [18] . We propose three possible explanations for why emissions have remained relatively flat despite an increase in O&G production. First, earlier federal regulations, namely NSPS Subpart OOOOa, instituted systematic Leak Detection and Repair (LDAR) for any O&G facility that was constructed, modified, or reconstructed after September 18, 2015 [19, 20] . These newer facilities are often built with cleaner equipment (e.g., air-driven pneumatics and controlled tanks) but have very high production volumes, contributing to lower intensity. Second, improvements to methane measurement technologies over the last decade have made it easier to detect large emissions, resulting in more opportunities for mitigation [21]. These improvements are especially important given that the largest emissions account for an outsized percentage of total methane emissions [22, 23] . Because these technological advancements occurred incrementally, we do not expect a precipitous drop in emissions in any one year from improved monitoring capabilities. Instead, these technological advancements, in aggregate, have likely contributed to the relatively flat emissions despite a substantial increase in production. Third, since 2019, rapid growth in U.S. liquefied natural gas (LNG) exports (see Figure S9) has driven a steady increase in the outflow of Permian Basin natural gas to global markets. The corresponding expansion of regional pipeline capacity has significantly reduced the flaring and direct venting of associated gas and is discussed in detail in the last section [24, 25].

Our estimated decrease in emissions intensity is relatively consistent with the emissions intensity trend in the EPA GHGI. Specifically, we estimate a decline of 11.2% [9.1%, 13.0%] from 2019 to 2022, falling from 10.1 [8.4, 10.8] to 9.0 [7.5, 9.7] 10^{-4} Tg $MMBOE^{-1}$, while the GHGI reports a 6.7% decline over the same period, falling

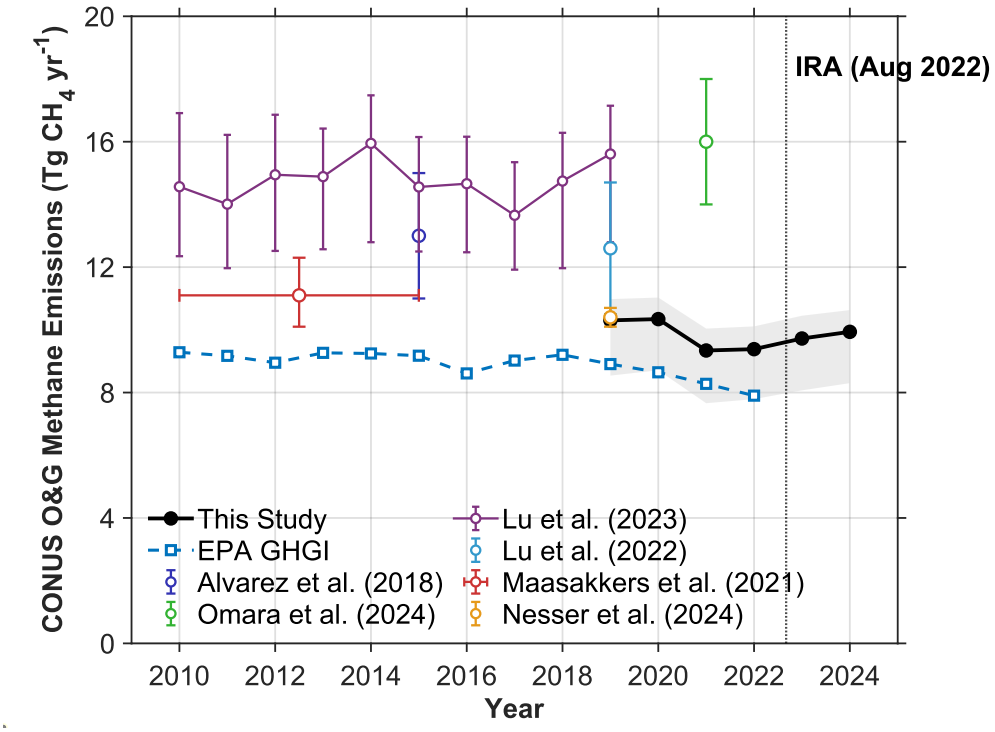


Fig. 2 CONUS O&G methane emission estimates during 2010–2024 [17, 26–30] . The black line represents the average of our O&G methane emission inverse model estimates, with the shaded area indicating the full range (minimum to maximum) of these values in 8 scenarios. The blue dashed line shows the official EPA Greenhouse Gas Inventory (GHGI) values we used within the inverse modeling prior. The vertical dotted line marks the enactment of the IRA in August 2022; notably, no detectable inflection point is observed in the emission trajectory following this policy intervention. Note that while some cited studies report total U.S. emissions, others focus on the CONUS and excludes Alaska and Hawaii. We argue that Alaska and Hawaii represent a negligible (∼1%) contribution to total anthropogenic methane emissions [28] and thus can be disregard for this comparison.

from 7.2 to 6.7 $\times$ 10^{-4} Tg MMBOE^{-1}. The EPA attributes this decline to pipeline replacement programs, improved materials and construction practices, enhanced leak detection and repair, and upgrades to transmission and storage infrastructure [31]. However, we find that total CONUS O&G methane emissions from 2019 to 2022 remained, on average, 17% higher than the GHGI (Fig. 2), a finding consistent with several independent top-down assessments of U.S. O&G emissions conducted over the past decade (2010 to 2021). Methane emissions estimates from these studies range from 10.4 to 18 Tg year^{-1}, values that are 33% to 100% higher than the EPA GHGI [17, 26–30]. The persistent discrepancy between these top-down assessments and the GHGI suggests that it may be capturing the right trend for the wrong reason, namely that it fundamentally underestimates emission magnitudes [32, 33]. Overall, our inverse

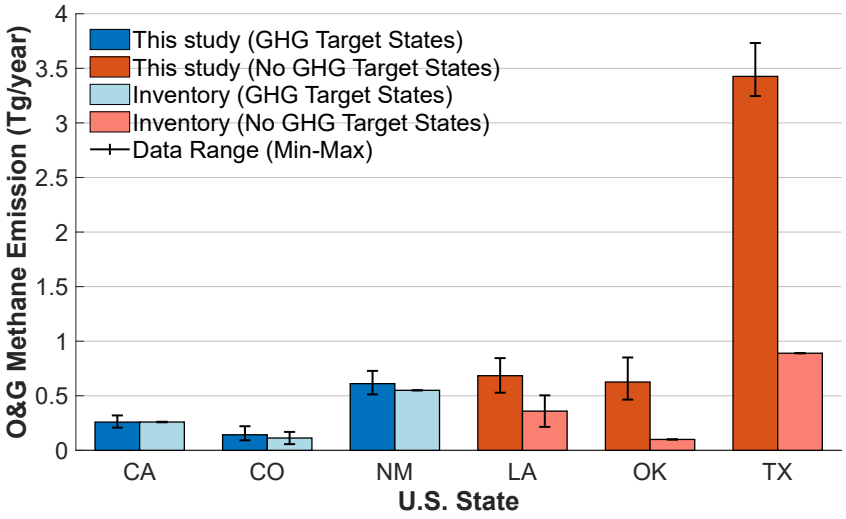


Fig. 3 Comparison of O&G methane emission estimates in three highest-emitting states with GHG reduction targets and those without GHG reduction targets derived from the inverse model and inventories during 2019–2024. Dark-colored bars represent average methane emissions estimated in our study (the O&G methane emission inverse model estimates), while light-colored bars represent average O&G methane emissions estimated using inventories (bottom-up) from California, Colorado, New Mexico, Louisiana, Oklahoma, and Texas during 2019–2024. Blue bars correspond to the three O&G methane-emitting states with GHG reduction targets, namely California, Colorado, and New Mexico, whereas red bars correspond to the three O&G methane-emitting states without GHG reduction targets, namely Louisiana, Oklahoma, and Texas. Black error bars indicate the full minimum-to-maximum range of available estimates for both inverse model and inventory methods during 2019–2024. Note that we only have inventory estimate for New Mexico in 2020, Oklahoma in 2020, and Texas in 2022.

model confirms that the GHGI provides a reliable directional trend on O&G methane emission intensity but likely underestimates O&G methane emissions.

Inventories from states with GHG targets are broadly consistent with inverse model estimates

State-level inventories exhibit varying degrees of agreement with our inverse modeling estimates, a divergence that correlates with the presence of state-level GHG emissions targets (see Table S2 for details of state-level GHG targets). We quantify this discrepancy using an emission ratio – defined as the inverse model estimate divided by the inventory estimate for each state. We focus on the three highest-emitting states with GHG reduction targets (New Mexico [34], California [35], Colorado [36]) and those without GHG reduction targets (Texas [37], Louisiana [38], Oklahoma [39]). For states with GHG reduction targets, inventory estimates for the O&G sector are broadly consistent with inverse model estimates, yielding a group average ratio of 1.1×. Specifically, California shows near-perfect agreement (1.0×), while Colorado (1.3×) and New Mexico (1.1×) remain closely aligned.

In contrast, for the three highest-emitting states without GHG targets, inventories for the O&G sector are substantially lower than inverse model estimates, with a group average ratio of 4.0×. This divergence is particularly acute in Texas (3.9×) and Oklahoma (6.3×). Such regional underestimation has persisted since Miller et al. [40] identified that total anthropogenic emissions in the South Central U.S. (Texas, Oklahoma, and Kansas) were $\sim 2.7\times$ higher than the Emissions Database for Global Atmospheric Research (EDGAR) inventories during 2007–2008, indicating that there is considerable potential for improvement in bottom-up reporting in regions lacking GHG emission targets. These findings also complement a recent study by Nesser et al. [28], who compared state-level emissions estimated from TROPOMI against the EPA's GHGI and against a handful of state inventories. The authors find that the GHGI underestimates emissions in most states. In contrast to the GHGI, we find that comparisons with state-level inventories are potentially more nuanced and correlate with the presence or absence of GHG targets, at least for the largest emitting states.

The discrepancy between these two groups of states could reflect multiple factors. First, states like California and Colorado fund methane measurements which may affect the accuracy of their inventories. For instance, the California Air Resources Board (CARB) has funded both methane measurements [41] and regional inverse modeling assessments to verify inventory accuracy [42–44]. Similarly, Colorado actively measures methane emissions from the O&G sector (e.g., the SABER and COBE campaigns [45]). Although these measurements are not always used to directly update state inventories, both Colorado and California often use customized emissions factors that are different from EPA's factors [46, 47]. By contrast, states like Texas and Oklahoma have generally lacked equivalent state-level investments in similar research programs to the same extent. Second, state inventories may underestimate emissions by applying emission factors derived from large, well-regulated facilities to smaller operators that fall below reporting thresholds. Instead of using direct measurements for these non-reporting sources, the emissions inventory in Texas [37] is estimated by linearly scaling based on production volumes. Similarly, Louisiana [38] and Oklahoma [39] rely on general calculation models, such as the EPA State Inventory Tool (SIT) and National Emissions Inventory (NEI), assuming that all facilities have the same emission intensity. This simplified approach does not reflect the fact that methane emissions intensity from low-producing oil wells are often disproportionately high [23, 48].

The relative accuracy of inventories in states with GHG targets does not, however, translate to guaranteed progress toward their reduction targets. For example, California's official inventory [49] reports that total anthropogenic methane emissions declined from 1.57 Tg CH_4 in 2013 to 1.45 Tg CH_4 in 2022. This modest 7.6% decline over 9 years in total anthropogenic emissions highlights a critical implementation gap. To satisfy the SB 1383 mandate of a 40% reduction by 2030, California must lower its annual emissions to 0.94 Tg yr^{-1}. This gap necessitates an additional reduction of 0.51 Tg before 2030 – a requirement that dwarfs the 0.12 Tg reduction achieved over the preceding decade. Our inverse model estimates further underscore this challenge: while California targets aggressive cuts, our inverse modeling estimate for California fluctuates around a multi-year average (1.5 ± 0.3 Tg during 2019–2024), suggesting that California would need to increase its methane emissions reductions to meet the

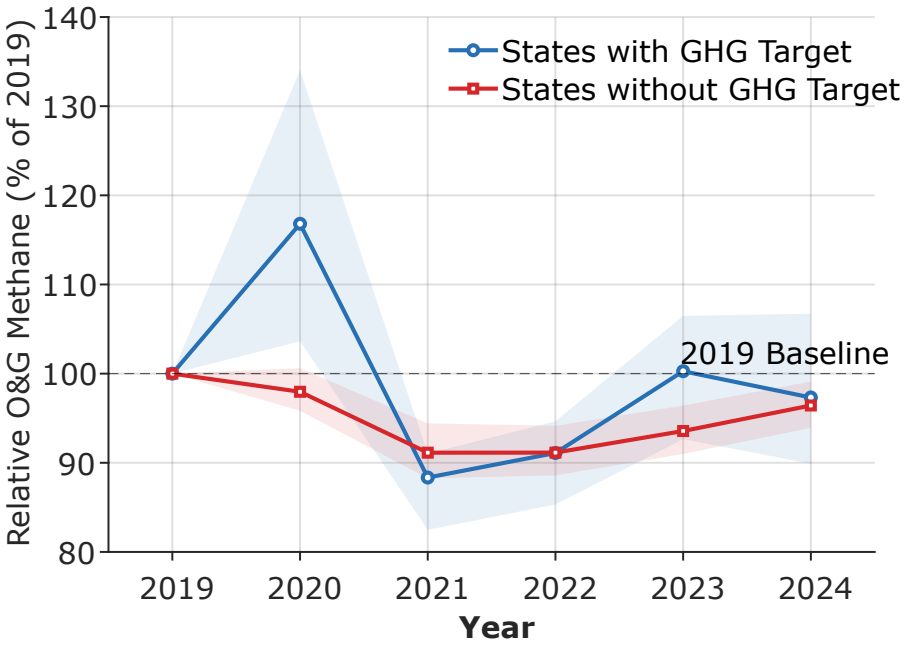


Fig. 4 Aggregated O&G methane emissions (Tg year^{-1}) for states with GHG reduction targets (blue) and without (red) GHG reduction targets (see Table S2 for the list of state with GHG target).

2030 statutory target. Similarly, Colorado faces significant hurdles in tracking its 2025 mandate to reduce methane emissions by 26% relative to 2005 levels. Our inverse model estimates for Colorado (2019–2024) show total anthropogenic emissions ranging from 0.39 to 0.97 Tg, with the O&G sector contributing 0.09–0.22 Tg. This variability is mirrored in the state's own inventory, which reports O&G methane emissions between 0.06 and 0.23 Tg during the 2021–2024 period. As a result, these structural uncertainties make it difficult to constrain the precise gap between Colorado's current levels and the 2025 target because the year-to-year variation (greater than 30%) exceed the state's methane emission reduction target (26%).

Interestingly, our inverse model ensemble (Fig. 4) reveals no substantial difference in O&G methane emission trends between states with and without GHG targets during 2019–2024. Specifically, the ensemble range of O&G methane emissions reduction rates for states with targets (1.03% to 2.57% yr^{-1}) overlaps with that of non-target states (0.60% to 1.49% yr^{-1}). This overlap suggests that the presence of state-level GHG targets alone was not a dominant driver of emission reductions in the short term. This lack of divergence is driven primarily by substantial emission reductions in major non-target states, most notably Texas. Texas – the largest emitting state – shows a 14% decline in O&G methane emissions in our inverse model from 3.73 Tg in 2019 to 3.24 Tg in 2024. The reason for this decline may relate to recent infrastructure changes in the state. Several gas pipelines were built across Texas between 2019 and

2024, so oil producers no longer need to flare co-produced gas and are instead able to send it to market via pipeline [50, 51]. Notably, the Gulf Coast Express (completed in late 2019) pipelines transports natural gas from the Permian Basin to Corpus Christi. Furthermore, the Whistler Express [52] and the newly commissioned Matterhorn Express Pipeline [53] transport Permian Basin natural gas to demand centers in the greater Houston area. Overall, the expansion of this infrastructure pipeline network may have led to a decrease in leaks and methane emissions [24, 25]. Also, the gas-to-oil ratio (GOR) in the Permian is increasing over time [54]. As a result, the gas produced is becoming more valuable, potentially incentivizing better infrastructure to process and transport gas. For example, existing studies have argued that oil-heavy basins tend to have higher methane emissions than gas-heavy basins [27]. These factors combined may have led to a decrease in O&G methane emissions in Texas despite increased O&G production and no GHG target.

Methods

Overview

The inverse model entails a two-step approach: a global inverse model for the first step and a higher-resolution regional inverse model for the second step. This approach is designed to ensure that regional emission estimates are physically consistent with global atmospheric constraints. Some existing studies use boundary conditions from other published work [55–57]; however, in this study, we use boundary conditions from the first step to ensure internal consistency.

The first step consists of a global inverse model to establish the boundary condition for the regional inverse model. We employ a mathematical framework similar to that of Chen et al. [58], but with modifications to the observations and predictor variables. In this step, we specifically run GEOS-Chem version 10-01b and the adjoint simulation version 36 at a 2° latitude by 2.5° longitude grid resolution. The 2° by 2.5° grid was chosen over smaller grids as a compromise to reduce the computing time required by GEOS-Chem and the inverse model. A single year of GEOS-Chem simulations typically requires 12 hours of wall-clock time on the Johns Hopkins University supercomputer (Rockfish). We run GEOS-Chem 50 times sequentially for each simulation year, resulting in a total computational investment of approximately 25 days to generate one year of global emissions estimates.

The second step is a regional inverse model focused on CONUS (23°N –51°N and 126.875°W–65.0°W). This step utilizes the optimized results from the global inverse model in the first step to define the essential initial conditions and boundary conditions. We specifically run GEOS-Chem version 10-01b and the adjoint simulation version 36 at a 0.5° latitude by 0.625° longitude grid resolution. A single year of regional GEOS-Chem simulations requires 7 hours of computing time on Rockfish. Following the 50-iteration sequential protocol, a year of regional inverse modeling requires approximately 15 days of computing time.

Observations

In both global and regional inverse models, we use the blended TROPOMI + GOSAT satellite data product for atmospheric methane [59]. The TROPOMI methane retrieval has numerous challenges with observational errors, and this blended product corrects TROPOMI observations to match the more accurate GOSAT methane retrievals [59]. Compared to the original TROPOMI L2 data, this product exhibits lower global biases relative to GOSAT, and it has been used in many studies [28, 55–57, 60, 61].

We select the 2019–2024 study period because blended TROPOMI + GOSAT satellite data became available starting May 2018. For the global inverse model (i.e., the first step described above), we begin our simulations at the beginning of the TROPOMI measurement period and discard the first eight months as a model warm-up. For the regional inverse model (i.e., the second step), we discard the first month as a model warm-up. The regional domain is initialized with the optimized methane mixing ratio fields and time-varying boundary conditions derived from the preceding global inverse model (the first step); thus, the regional model (the second step) reaches physical and chemical equilibrium rapidly. We also evaluate our inverse modeling results using in-situ observations (in CONUS only) from the National Oceanic and Atmospheric Administration (NOAA) Observation Package (ObsPack) dataset (obspack_ch4_1_GLOBALVIEWplus_v6.0_2023-12-01) [62]. We do not use these in-situ observations to constrain methane emissions within the inverse model but rather use them as independent data for evaluating the inverse model.

Inverse model

In both the global and regional inverse models, we use the same underlying mathematical equations. For the setup here, we have n TROPOMI observations collected across different times and locations and aim to estimate unknown emissions in m model grid boxes at different locations and on different days (where n and m have different values in the global and regional models) [58, 63, 64]:

$$\boldsymbol{z} = \boldsymbol{h}(\boldsymbol{s}) + \boldsymbol{\epsilon} \tag{1}$$

where $\boldsymbol{z}$ represents the TROPOMI methane observations (dimensions $n \times 1$, in ppb). For example, for the global inverse model, we use approximately 200,000 TROPOMI observations every day over 610 days (20 months). Therefore, $n \approx 610 \times 200,000$ for the global simulations. Similarly, $n \approx 395 \times 2,000$ for the regional inverse model (395 days = 13 months). The function $\boldsymbol{h}()$ represents the atmospheric transport model, and $\boldsymbol{s}$ is the vector of methane emissions to be estimated (dimensions $m \times 1$, in units of kg m^{-2} s^{-1}). For the global inverse model, we have 4,219 model grids each day over the 610 day study period. Therefore, $m = 610 \times 4,219 = 2,573,590$. Similarly, $m = 395 \times 5,700 = 2,251,500$ for the regional inverse model. In addition, the variable $\boldsymbol{\epsilon}$ represents the model-data mismatch errors, which include errors in the measurements and the atmospheric transport model ($n \times 1$) [65]:

$$\boldsymbol{\epsilon} \sim \mathcal{N}(0, \mathbf{R})$$

where the symbol $\sim$ means "is distributed as", $\mathcal{N}$ is a multivariate normal or Gaussian distribution. $\mathbf{R}$ $(n \times n)$ is a covariance matrix that characterizes the properties of the errors ($\boldsymbol{\epsilon}$), and we need to estimate these properties before running the inverse model. In both global and regional inverse models, we set the diagonal elements of $\mathbf{R}$ equal to $(25 \text{ ppb})^2$ same as previous work [58]. We also tested $(15 \text{ ppb})^2$ in some scenarios (see Table 1). We also require an initial condition or restart file that provides methane mixing ratios in the global atmosphere on the first day of our simulations, and we use estimates of methane mixing ratios from the CAMS global GHG reanalysis (EGG4), downloaded from the Copernicus Atmosphere Monitoring Service (CAMS) Atmosphere Data Store (ADS) for the global inverse model [66]. We use estimates from the global inverse modeling simulations as the initial condition and boundary condition for regional inverse modeling simulations.

Using these inputs, the inverse model will estimate emissions $\boldsymbol{s}$ that consist of two components: a deterministic component $\mathbf{X}\boldsymbol{\beta}$ and a stochastic component $\boldsymbol{\zeta}$. The emissions ($\boldsymbol{s}$) and coefficients ($\boldsymbol{\beta}$) are estimated simultaneously in the setup here, and the stochastic component $\boldsymbol{\zeta}$ is subsequently straightforward to calculate [63, 65]:

$$\boldsymbol{s} = \mathbf{X}\boldsymbol{\beta} + \boldsymbol{\zeta} \tag{2}$$

where $\mathbf{X}$ is a matrix of predictor variables (dimensions $m \times p$, and $p = 1$). These predictor variables can encompass any product or dataset that helps predict the spatial and temporal distribution of methane emissions. In this study, we use emissions inventories in $\mathbf{X}$, but existing studies of methane emissions that use the same inverse modeling equations (Eq. 1 and Eq. 2) have sometimes used more creative predictor variables, including directly assimilating soil carbon maps, wetland maps, and maps of agricultural activities [40, 67, 68]. The inverse model will estimate coefficients ($\boldsymbol{\beta}$) that scale the magnitude of these predictor variables to produce the best match possible against atmospheric methane observations (Eq. 1). The inverse model will also estimate grid-scale patterns in the emissions ($\boldsymbol{\zeta}$) that cannot be described by any of the available predictor variables. In other words, the stochastic component will correct the spatial and temporal patterns in the deterministic model, so that the estimated emissions better match the observations. The inverse model uses a covariance matrix $\mathbf{Q}$ (dimensions $m \times m$) to guide the properties of $\boldsymbol{\zeta}$, and the parameters that define $\mathbf{Q}$ must be prescribed by the modeler:

$$\boldsymbol{\zeta} \sim \mathcal{N}(0, \mathbf{Q}),$$

The diagonal elements of $\mathbf{Q}$ define the variance of $\boldsymbol{\zeta}$ in space and time, and the off-diagonal elements prescribe spatial and temporal correlations in $\boldsymbol{\zeta}$. We set the diagonal elements of $\mathbf{Q}$ to $(1 \times 10^{-10} \text{ kg m}^{-2} \text{ s}^{-1})^2$, the same as Chen et al. [58]. We use this value because the standard deviation of the bottom-up estimates (i.e., predictor variables) in $\mathbf{X}$ is approximately 1×10^{-10} kg m^{-2} s^{-1}. We also tested 2×10^{-10} kg m^{-2} s^{-1} in some scenarios (see Table 1). Hence, we allow the stochastic component of the inverse model to make corrections to the bottom-up estimates (i.e., predictor variables) that are similar in magnitude to those estimates. We further set the de-correlation length to 500 km or 200 km (using a spherical model), and we set the

de-correlation time of the stochastic component to 30 days or 90 days, similar to previous work [40, 69]. Previous inverse modeling studies often set a de-correlation length of 100 km to 500 km [40, 69–72]).

We estimate the emissions using the L-BFGS optimization algorithm, following the approach described in Miller et al. [64]. In addition, we use a square root transformation to ensure that the resulting emissions estimate is not negative (see SI for more details about the L-BFGS method). Although natural soils provide a small global methane sink, the anthropogenic emission categories optimized in our study are strictly positive sources. Enforcing a non-negativity constraint is therefore critical to preventing the optimization algorithm from generating physically unrealistic sinks to mathematically compensate for localized transport errors. Consequently, non-negativity constraint is widely adopted in previous studies [40, 55, 73].

Predictor variables

For the global inverse model, we use predictor variables similar to our previous work [58], and for the regional inverse model, we run simulations with 2 anthropogenic and 2 wetland models (see Table 1). We use multiple simulations to ensure that the posterior emissions from the inverse model are not unduly influenced by a single, subjectively chosen predictor variable. Note that we sum these different emissions products (including one anthropogenic and one wetland product for each inverse modeling run) into a single predictor variable, so $\mathbf{X}$ in this study only has a single column. We subsequently solve for total methane emissions in the inverse model and later derive estimates for O&G methane emissions (described in the next section).

We combine multiple global and regional inventories for anthropogenic emissions. Specifically, we use the default regional and global emissions inventories in the Harmonized Emissions Component (HEMCO) version 3.9.0 [74]. Note that HEMCO is a software module that re-grids and combines emissions from various regional and global inventories (e.g., EDGAR) into GEOS-Chem. The global inventory includes the Global Fuel Exploitation Inventory version 2.0 [75] for the oil, gas, and coal sectors, Global Fire Emissions Database version 4 (GFEDv4) for biomass burning emissions, reservoir emissions [76], and the EDGAR v8 inventory [77] for other anthropogenic sources. Regional inventories include the Inventory of U.S. Greenhouse Gas Emissions and Sinks (GHGI) [78] for the U.S., as well as regional inventories for Canada [79] and Mexico [80]. For global inverse modeling simulations, regional inventories (e.g., GHGI) override global inventories (e.g., EDGAR) in their respective domains. For the regional inverse model, we use EDGAR in some scenarios and GHGI in others. For wetland methane emissions, we use the mean from the Global Carbon Project (GCP) process-based model ensemble [81] in some scenarios and the average of the WetCHARTs (another ensemble of wetland models) [82] in others.

Inverse modeling scenarios

In total, we conduct 8 different regional inverse modeling scenarios for each year (over five years), each using different predictor variables for wetland emissions and anthropogenic emissions. We present the average of these 8 simulations throughout the

results. We also present the ensemble range of these 8 scenarios in the results but we note that this ensemble range is not the same as the posterior uncertainties. Rather, it captures some of the uncertainties related to the predictor variables and observational errors. By contrast, the L-BFGS method does not provide a mathematical estimate of the posterior uncertainty. To evaluate the sensitivity of our inverse model estimates to OH uncertainties, we perform additional simulations with global OH concentrations reduced by 1.6% [83] and 4.0% [84] in 2020 (see SI).

The 8 different scenarios are outlined in the table below.

Table 1 Overview of scenarios used in this study.

Scenario	Initial Conditions	Warm-up	Wetland	Anthropogenic	Parameters*
1	CAMS	8 months	WetCHARTs	EDGAR v8	1, 25, 30, 500
2	CAMS	8 months	GCP	GHGI	1, 25, 30, 500
3	Chen et al. (2025)	1 month	WetCHARTs	EDGAR v8	1, 25, 30, 500
4	Chen et al. (2025)	1 month	GCP	GHGI	1, 25, 30, 500
5	Chen et al. (2025)	1 month	WetCHARTs	EDGAR v8	1, 15, 30, 500
6	Chen et al. (2025)	1 month	WetCHARTs	EDGAR v8	2, 25, 30, 500
7	Chen et al. (2025)	1 month	WetCHARTs	EDGAR v8	1, 25, 90, 500
8	Chen et al. (2025)	1 month	WetCHARTs	EDGAR v8	1, 15, 30, 200

*The column "Parameters" lists the hyperparameters in the following order:
1. Square root of the diagonal elements of $\mathbf{Q}$ (unit: 10^{-10} kg m^{-2} s^{-1});
2. Square root of the diagonal elements of $\mathbf{R}$ (unit: ppb);
3. De-correlation time (unit: days);
4. De-correlation length (unit: km).
Scenarios 5–8 represent sensitivity tests with perturbed parameters relative to the baseline (Scenario 3).

The posterior emissions from the inverse model ($\boldsymbol{s}$) provide an estimate of total methane emissions in each model grid box, not emissions for individual source types (e.g., oil sector and gas sector). Hence, we need an approach to estimate sectoral emissions from O&G sources. We first calculate the fraction of emissions in each grid box that are attributable to O&G using existing inventories and bottom-up models. For this calculation, we use anthropogenic emissions from EDGAR (or GHGI), biomass burning emissions from GFED, and wetland emissions from the average of the GCP (or WetCHARTs) model ensemble. We subsequently multiply our posterior emissions estimate in each grid box by the corresponding fraction calculated in the previous step. We sum this O&G contribution across individual regions or across the globe to obtain O&G emission totals. This method has been used in several existing inverse modeling studies [58, 70, 72, 85, 86]. It is important to note, however, that the attribution of emissions to specific sources introduces additional uncertainty in the posterior emissions estimate. Specifically, the approach used here relies on the ratio of anthropogenic versus wetland emissions in existing bottom-up estimates, and errors in this ratio (e.g., EDGAR, GHGI, GCP, and WetCHARTs) could propagate into errors in the estimated source attribution. Fortunately, this approach to attribution does not assume that the absolute magnitude of emissions in the bottom-up models is correct.

Acknowledgments

We thank Nicholas Balasus for the blended TROPOMI+GOSAT satellite data product. We also thank the ObsPack team at NOAA and collaborating organizations for providing in situ observations. This work contains modified Copernicus Climate Change Service information 2025, downloaded from the Copernicus Atmosphere Monitoring Service (CAMS) Atmosphere Data Store (ADS) (https://ads.atmosphere.copernicus.eu/cdsapp#!/dataset/cams-global-ghg-reanalysis-egg4?tab=form). Neither the European Commission nor ECMWF is responsible for any use that may be made of the Copernicus information or data it contains. We further thank the HEMCO teams for providing emissions inventories and software for computing atmospheric emissions. We also thank the Sentinel-5P TROPOMI Methane team for the satellite dataset. We further thank Benjamin Hobbs and Julie McDill for their helpful discussions regarding this paper. This work is funded by an NSF CAREER award (#2237404).

References

[1] EPA. Waste Emissions Charge (2025). URL https://www.epa.gov/inflation-reduction-act/waste-emissions-charge.

[2] Larsen, J. *et al.* Energy & Climate A Turning Point for US Climate Progress: Assessing the Climate and Clean Energy Provisions in the Inflation Reduction Act. Tech. Rep., Rhodium Group (2022).

[3] EPA. Methane Emissions Reduction Program (2024). URL https://www.epa.gov/inflation-reduction-act/methane-emissions-reduction-program.

[4] Executive Office of the President. Executive Order 13990: Protecting Public Health and the Environment and Restoring Science To Tackle the Climate Crisis. 86 FR 7037 (2021). URL https://www.federalregister.gov/documents/2021/01/25/2021-01765/protecting-public-health-and-the-environment-and-restoring-science-to-tackle-the-climate-crisis.

[5] Environmental Protection Agency. Standards of Performance for New, Reconstructed, and Modified Sources and Emissions Guidelines for Existing Sources: Oil and Natural Gas Sector Climate Review. 89 FR 16820 (2024). URL https://www.federalregister.gov/documents/2024/03/08/2024-00366/standards-of-performance-for-new-reconstructed-and-modified-sources-and-emissions-guidelines-for.

[6] Environmental & Energy Law Program, Harvard Law School. EPA VOC and Methane Standards for Oil and Gas Facilities. Regulatory Tracker (2026). URL https://eelp.law.harvard.edu/tracker/epa-voc-and-methane-standards-for-oil-and-gas-facilities-2/. Last updated: February 24, 2026.

[7] Ramseur, J. L. Inflation Reduction Act Methane Emissions Charge: Overview and Developments. CRS Report R48475, Congressional Research Service (2025). URL https://www.congress.gov/crs-product/R48475.

[8] U.S. Environmental Protection Agency. President Trump and Administrator Zeldin Deliver Single Largest Deregulatory Action in U.S. History. Press Release (2026). URL https://www.epa.gov/newsreleases/president-trump-and-administrator-zeldin-deliver-single-largest-deregulatory-action-us.

[9] Shields, L. Greenhouse Gas Emissions Reduction Targets and Market-based Policies. National Conference of State Legislatures (NCSL) Report (2023). URL https://www.ncsl.org/energy/greenhouse-gas-emissions-reduction-targets-and-market-based-policies.

[10] Hultman, N. E. *et al.* Fusing subnational with national climate action is central to decarbonization: the case of the United States. *Nature Communications* **11**, 5255 (2020).

[11] U.S. Energy Information Administration. U.S. Field Production of Crude Oil. Petroleum & Other Liquids Database (2026). URL https://www.eia.gov/dnav/pet/hist/LeafHandler.ashx?n=pet&s=mcrfpus2&f=a. Accessed: 2026-03-31.

[12] Ramseur, J. L. Inflation Reduction Act Methane Emissions Charge: In Brief. CRS Report R47206, Congressional Research Service (2022). URL https://www.congress.gov/crs-product/R47206.

[13] U.S. Environmental Protection Agency. Regulatory Impact Analysis of the Proposed Waste Emissions Charge. Tech. Rep. EPA-452/R-24-001, U.S. Environmental Protection Agency (2024). URL https://www.epa.gov/system/files/documents/2024-01/wec_ria.pdf. Office of Air Quality Planning and Standards.

[14] U.S. Environmental Protection Agency. Regulatory Impact Analysis of the Standards of Performance for New, Reconstructed, and Modified Sources and Emissions Guidelines for Existing Sources: Oil and Natural Gas Sector Climate Review. Tech. Rep., U.S. Environmental Protection Agency (2023). URL https://www.epa.gov/system/files/documents/2023-12/eo12866_oil-and-gas-nsps-eg-climate-review-2060-av16-ria-20231130.pdf. EPA-452/R-23-016.

[15] Oil and Gas Climate Initiative (OGCI). OGCI publishes its Reporting Framework for 2024 data on emissions. OGCI news (2024). URL https://www.ogci.com/news/ogci-publishes-its-reporting-framework-for-2024-data-on-emissions/. Accessed: 2026-03-31.

[16] Kathairos Solutions. News Update: The Oil Industry is Bracing for the Methane Fee. Here's What to Know. Dick Brown (2024). URL https://www.kathairos.com/news/news-oil-industry-methane-fee. September 9, 2024.

[17] Lu, X., Jacob, D. J., Zhang, Y., Fan, S. *et al.* Observation-derived 2010–2019 trends in methane emissions and intensities from US oil and gas fields tied to activity metrics. *Proceedings of the National Academy of Sciences (PNAS)* **120**, e2217900120 (2023). URL https://www.pnas.org/doi/10.1073/pnas.2217900120.

[18] Varon, D. J. *et al.* Seasonality and Declining Intensity of Methane Emissions from the Permian and Nearby US Oil and Gas Basins. *Environmental Science & Technology* **60** (2025). URL https://pubs.acs.org/doi/10.1021/acs.est.5c08745.

[19] National Archives. Code of Federal Regulations, Title 40, Protection of Environment, Part 60. Electronic Code of Federal Regulations (eCFR) (2026). URL https://www.ecfr.gov/current/title-40/chapter-I/subchapter-C/part-60. Accessed: March 27, 2026.

[20] LaCount, R., Curry, T., Hellgren, L. & Russell, P. Benchmarking Methane and Other GHG Emissions of Oil & Natural Gas Production in the United States. Tech. Rep., Clean Air Task Force and Ceres (2021). URL https://www.catf.us/

wp-content/uploads/2021/06/OilandGas_BenchmarkingReport_FINAL.pdf. Data available at www.mjbradley.com.

[21] Fox, T. A., Barchyn, T. E., Risk, D., Ravikumar, A. P. & Hugenholtz, C. H. A review of close-range and screening technologies for mitigating fugitive methane emissions in upstream oil and gas. *Environmental Research Letters* **14**, 053002 (2019). URL https://iopscience.iop.org/article/10.1088/1748-9326/ab0cc3.

[22] Brandt, A. R., Heath, G. A. & Cooley, D. Methane leaks from natural gas systems follow extreme distributions. *Environmental Science & Technology* **50**, 12512–12520 (2016). URL https://pubs.acs.org/doi/10.1021/acs.est.6b04303.

[23] Omara, M. *et al.* Methane emissions from US low production oil and natural gas well sites. *Nature Communications* **13**, 2085 (2022). URL https://www.nature.com/articles/s41467-022-29709-3.

[24] Lyon, D. R. *et al.* Concurrent variation in oil and gas methane emissions and price during the COVID-19 pandemic. *Atmospheric Chemistry and Physics* **21**, 6605–6626 (2021). URL https://acp.copernicus.org/articles/21/6605/2021/.

[25] Zhang, Y. *et al.* Quantifying methane emissions from the largest oil-producing basin in the United States from space. *Science Advances* **6**, eaaz5120 (2020). URL https://www.science.org/doi/10.1126/sciadv.aaz5120.

[26] Maasakkers, J. D. *et al.* 2010–2015 North American methane emissions, sectoral contributions, and trends: a high-resolution inversion of GOSAT observations of atmospheric methane. *Atmospheric Chemistry and Physics* **21**, 4339–4356 (2021). URL https://doi.org/10.5194/acp-21-4339-2021.

[27] Omara, M. *et al.* Constructing a measurement-based spatially explicit inventory of US oil and gas methane emissions (2021). *Earth System Science Data* **16**, 3973–3991 (2024). URL https://doi.org/10.5194/essd-16-3973-2024.

[28] Nesser, H. *et al.* High-resolution US methane emissions inferred from an inversion of 2019 TROPOMI satellite data: contributions from individual states, urban areas, and landfills. *Atmospheric Chemistry and Physics* **24**, 5069–5091 (2024). URL https://acp.copernicus.org/articles/24/5069/2024/.

[29] Alvarez, R. A. *et al.* Assessment of methane emissions from the U.S. oil and gas supply chain. *Science* **361**, 186–188 (2018). URL https://doi.org/10.1126/science.aar7204.

[30] Shen, L. *et al.* Satellite quantification of oil and natural gas methane emissions in the US and Canada including contributions from individual basins. *Atmospheric Chemistry and Physics* **22**, 11203–11215 (2022). URL https://doi.org/10.5194/acp-22-11203-2022.

[31] U.S. Environmental Protection Agency. Inventory of U.S. Greenhouse Gas Emissions and Sinks: 1990–2022. Tech. Rep. EPA 430-R-24-004, U.S. Environmental Protection Agency (2024). URL https://www.epa.gov/ghgemissions/inventory-us-greenhouse-gas-emissions-and-sinks-1990-2022.

[32] Helmig, D. & Caputi, D. Top-Down versus bottom-up atmospheric emission estimates from oil and natural gas operations. *Earth's Future* (2025). URL https://agupubs.onlinelibrary.wiley.com/doi/10.1029/2025EF006534.

[33] Brandt, A. R. *et al.* Methane leaks from North American natural gas systems. *Science* **343**, 733–735 (2014). URL https://www.science.org/doi/10.1126/science.1247045.

[34] New Mexico Environment Department. New Mexico Oil and Gas Greenhouse Gas Emissions Inventory for Year 2020. Tech. Rep., Colorado State University, Center for the New Energy Economy (2022). URL https://cloud.env.nm.gov/resources/_translator.php/YjMwMmZhMWY5NjEwMGMyMWQwZDkzODk5NV8xNzc2NjE~.pdf. Prepared for the New Mexico Environment Department.

[35] California Air Resources Board. California Greenhouse Gas Inventory for 2000-2023 (2025). URL https://ww2.arb.ca.gov/sites/default/files/2025-11/nc-ghg_inventory_ipcc_sum_00-23_CH4.xlsx. Accessed: 2026-03-31.

[36] Colorado Department of Public Health & Environment. Oil and Gas Annual Emissions Inventory Dashboard: Trends. Interactive Data Visualization (2026). URL https://cohealthviz.dphe.state.co.us/t/APCDPublic/views/OilandGasAnnualEmissionsInventoryDashboard/Trends. Air Pollution Control Division (APCD) Public Portal. Accessed: 2026-03-31.

[37] Allen, D. *et al.* Greenhouse Gas Inventory for Texas. Tech. Rep., University of Texas at Austin, Center for Energy and Environmental Systems Analyses (2024). URL https://www.tceq.texas.gov/downloads/agency/climate-pollution-reduction-grants/2022-texas-greenhouse-gas-inventory.pdf. Prepared for Texas Commission on Environmental Quality (TCEQ) under the Climate Pollution Reduction Grants Program.

[38] Dismukes, D. E. Louisiana 2021 Greenhouse Gas Inventory. Tech. Rep., LSU Center for Energy Studies (2021). URL https://www.lsu.edu/ces/publications/2021/louisiana-2021-greehouse-gas-inventory-df-rev_reduced.pdf. Prepared on behalf of the Governor's Office of Coastal Activities.

[39] Oklahoma Department of Environmental Quality. State Emissions Totals and Infographics. Air Quality Division (2026). URL https://oklahoma.gov/deq/divisions/air-quality/emissions-inventory/state-emissions-totals-infographics.html. Accessed: 2026-03-31.

[40] Miller, S. M. *et al.* Anthropogenic emissions of methane in the United States. *Proceedings of the National Academy of Sciences of the United States of America* **110**, 20018–20022 (2013).

[41] California Energy Commission. The California Methane Survey. Tech. Rep. CEC-500-2020-047, California Energy Commission (2020). URL https://www.energy.ca.gov/publications/2020/california-methane-survey. Gas Research and Development Program.

[42] Zhao, C. *et al.* Atmospheric inverse estimates of methane emissions from Central California. *Journal of Geophysical Research: Atmospheres* **114**, D16302 (2009). URL https://doi.org/10.1029/2008JD011671.

[43] Jeong, S. *et al.* A multitower measurement network estimate of California's methane emissions. *Journal of Geophysical Research: Atmospheres* **118**, 11,339–11,351 (2013). URL https://doi.org/10.1002/jgrd.50854.

[44] Jeong, S. *et al.* Estimating methane emissions in California's urban and rural regions using multitower observations. *Journal of Geophysical Research: Atmospheres* **121**, 13,031–13,049 (2016). URL https://doi.org/10.1002/2016JD025404.

[45] Colorado Department of Public Health & Environment. Greenhouse gas monitoring projects, reports, and data (2026). URL https://cdphe.colorado.gov/greenhouse-gas-monitoring-projects-reports-and-data. Accessed: 2026-03-31.

[46] Ersoy, D. & Adamo, M. Quantifying Methane Emissions from Distribution Pipelines in California. Final Report ARB Agreement Number: 12-420, California Air Resources Board (2021). URL https://ww2.arb.ca.gov/sites/default/files/2021-01/Final_CARB_Pipeline_Study_1-14-21.pdf. GTI Project No. 22504.

[47] Colorado Department of Public Health & Environment. Oil and Natural Gas Annual Emission Inventory Reporting (2026). URL https://cdphe.colorado.gov/ongaeir. Accessed: 2026-03-31.

[48] Deighton, J. A., Townsend-Small, A., Sturmer, S. J., Hoschouer, J. & Heldman, L. Measurements show that marginal wells are a disproportionate source of methane relative to production. *Journal of the Air & Waste Management Association* **70**, 1030–1042 (2020). URL https://doi.org/10.1080/10962247.2020.1808115.

[49] California Air Resources Board. AB 32 GHG Emissions Inventory 2024 Edition Documents (2024). URL https://ww2.arb.ca.gov/resources/documents/ab-32-ghg-emissions-inventory-2024-edition-documents. Accessed: 2026-03-31.

[50] Allen, D. T., Roman-White, S. A., McCormick, M. & George, F. Moving toward zero routine flaring in the Permian Basin oil and gas production region: measuring progress and driving factors. *ACS Sustainable Resource Management* **1** (2024). URL https://pubs.acs.org/doi/10.1021/acssusresmgt.4c00091.

[51] U.S. Energy Information Administration. Permian production forecast growth driven by well productivity, pipeline capacity. Today in Energy (2024). URL https://www.eia.gov/todayinenergy/detail.php?id=62884. Accessed: 2026-03-31.

[52] U.S. Energy Information Administration. New natural gas pipeline capacity expands access to export and Northeast markets. Today in Energy (2021). URL https://www.eia.gov/todayinenergy/detail.php?id=50376. Accessed: 2026-03-31.

[53] Matterhorn Express Pipeline. About Us: Project Overview (2026). URL https://matterhornexpress.com/. Accessed: 2026-03-31.

[54] U.S. Energy Information Administration. Associated natural gas production has tripled since 2018 in top three Permian oil plays. Today in Energy (2023). URL https://www.eia.gov/todayinenergy/detail.php?id=61043. Accessed: 2026-03-31.

[55] Hancock, S. E. *et al.* Satellite quantification of methane emissions from South American countries: a high-resolution inversion of TROPOMI and GOSAT observations. *Atmospheric Chemistry and Physics* **25**, 797–817 (2025).

[56] Sicsik-Paré, A. *et al.* Can we obtain consistent estimates of the emissions in europe from three different ch4 tropomi products? *EGUsphere* (2025). URL https://egusphere.copernicus.org/preprints/2025/egusphere-2025-2622/.

[57] East, J. D. *et al.* Interpreting the seasonality of atmospheric methane. *Geophysical Research Letters* **51** (2024).

[58] Chen, A. *et al.* Spatial and temporal distribution of global wetland methane emissions during 2019–2020 estimated from satellite observations. *Journal of Geophysical Research: Atmospheres* **130** (2025).

[59] Balasus, N. *et al.* A blended TROPOMI+GOSAT satellite data product for atmospheric methane using machine learning to correct retrieval biases. *Atmospheric Measurement Techniques* **16**, 3787–3807 (2023).

[60] Balasus, N. *et al.* Satellite monitoring of annual US landfill methane emissions and trends. *Environmental Research Letters* **20** (2025).

[61] Pendergrass, D. C. *et al.* Trends and seasonality of 2019–2023 global methane emissions inferred from a localized ensemble transform kalman filter (cheereio v1.3.1) applied to tropomi satellite observations. *Atmospheric Chemistry and Physics* **25**, 14353–14369 (2025).

[62] Schuldt, K. N. *et al.* Multi-laboratory compilation of atmospheric methane data for the years 2020-2021; obspack_ch4_1_NRT_v3.0_2021-05-18 [dataset] (2021).

[63] Michalak, A. M., Bruhwiler, L. & Tans, P. P. A geostatistical approach to surface flux estimation of atmospheric trace gases. *Journal of Geophysical Research:*

Atmospheres **109** (2004).

[64] Miller, S. M., Saibaba, A. K., Trudeau, M. E., Mountain, M. E. & Andrews, A. E. Geostatistical inverse modeling with very large datasets: An example from the Orbiting Carbon Observatory 2 (OCO-2) satellite. *Geoscientific Model Development* **13**, 1771–1785 (2020).

[65] Kitanidis, P. K. & Vomvoris, E. G. A geostatistical approach to the inverse problem in groundwater modeling (steady state) and one-dimensional simulations. *Water Resources Research* **19**, 677–690 (1983).

[66] Inness, A. *et al.* CAMS global reanalysis (EAC4). Copernicus Atmosphere Monitoring Service (CAMS) Atmosphere Data Store (ADS). (Accessed on 03-Mar-2025) [dataset] (2019).

[67] Miller, S. M. *et al.* Observational constraints on the distribution, seasonality, and environmental predictors of North American boreal methane emissions. *Global Biogeochemical Cycles* **28**, 146–160 (2014).

[68] Miller, S. M. *et al.* A multiyear estimate of methane fluxes in Alaska from CARVE atmospheric observations. *Global Biogeochemical Cycles* **30**, 1441–1453 (2016).

[69] Monteil, G. *et al.* Comparison of CH_4 inversions based on 15 months of GOSAT and SCIAMACHY observations. *Journal of Geophysical Research Atmospheres* **118**, 807–11 (2013).

[70] Wecht, K. J., Jacob, D. J., Frankenberg, C., Jiang, Z. & Blake, D. R. Mapping of North American methane emissions with high spatial resolution by inversion of SCIAMACHY satellite data. *Journal of Geophysical Research: Atmospheres* **119**, 7741–7756 (2014).

[71] Yu, X. *et al.* Aircraft-based inversions quantify the importance of wetlands and livestock for Upper Midwest methane emissions. *Atmospheric Chemistry and Physics* **21**, 951–971 (2021).

[72] Yu, X. *et al.* A high-resolution satellite-based map of global methane emissions reveals missing wetland, fossil fuel, and monsoon sources. *Atmospheric Chemistry and Physics* **23**, 3325–3346 (2023).

[73] Chen, Z. *et al.* Satellite quantification of methane emissions and oil-gas methane intensities from individual countries in the Middle East and North Africa: implications for climate action. *Atmospheric Chemistry and Physics* **23**, 5945–5967 (2023).

[74] Lin, H. *et al.* Harmonized Emissions Component (HEMCO) 3.0 as a versatile emissions component for atmospheric models: Application in the GEOS-Chem, NASA GEOS, WRF-GC, CESM2, NOAA GEFS-Aerosol, and NOAA UFS models.

Geoscientific Model Development **14**, 5487–5506 (2021).

[75] Scarpelli, T. R. *et al.* Updated Global Fuel Exploitation Inventory (GFEI) for methane emissions from the oil, gas, and coal sectors: Evaluation with inversions of atmospheric methane observations. *Atmospheric Chemistry and Physics* **22** (2022).

[76] Delwiche, K. B. *et al.* Estimating driver and pathways for hydroelectric reservoir methane emissions using a new mechanistic model. *Journal of Geophysical Research: Biogeosciences* **127** (2022).

[77] Crippa, M. *et al.* EDGAR v8.0 greenhouse gas emissions. European Commission, Joint Research Centre (JRC) (2023).

[78] Maasakkers, J. D. *et al.* A gridded inventory of annual 2012-2018 U.S. anthropogenic methane Emissions. *Environmental Science and Technology* **57**, 16276–16288 (2023).

[79] Scarpelli, T. R., Jacob, D. J., Moran, M., Reuland, F. & Gordon, D. A gridded inventory of Canada's anthropogenic methane emissions. *Environmental Research Letters* **17** (2022).

[80] Scarpelli, T. R. *et al.* A gridded inventory of anthropogenic methane emissions from Mexico based on Mexico's national inventory of greenhouse gases and compounds. *Environmental Research Letters* **15** (2020).

[81] Zhang, Z. *et al.* Ensemble estimates of global wetland methane emissions over 2000–2020. *Biogeosciences* **22**, 305–321 (2025).

[82] Bloom, A. A. *et al.* A global wetland methane emissions and uncertainty dataset for atmospheric chemical transport models (WetCHARTs version 1.0). *Geoscientific Model Development* **10**, 2141–2156 (2017).

[83] Peng, S. *et al.* Wetland emission and atmospheric sink changes explain methane growth in 2020. *Nature* **612**, 477–482 (2022).

[84] Chen, W., Zhang, Y. & Liang, R. Converging evidence for reduced global atmospheric oxidation in 2020. *National Science Review* **12**, nwaf232 (2025). URL https://doi.org/10.1093/nsr/nwaf232.

[85] Miller, S. M. *et al.* China's coal mine methane regulations have not curbed growing emissions. *Nature Communications* **10** (2019).

[86] Qu, Z. *et al.* Inverse modeling of 2010–2022 satellite observations shows that inundation of the wet tropics drove the 2020–2022 methane surge. *Proceedings of the National Academy of Sciences* **121** (2024).

Supplementary Files

This is a list of supplementary files associated with this preprint. Click to download.

- SI.pdf